G. SIDENIUS

SYSTEMATIC STOPPING CROSS SECTION MEASUREMENTS WITH LOW ENERGY IONS IN GASES

Det Kongelige Danske Videnskabernes Selskab
Matematisk-fysiske Meddelelser **39**, 4

Kommissionær: Munksgaard
København 1974

Synopsis

Systematic stopping cross sections were measured in Methane (CH_4) for particles with atomic number $Z_1 \leq 10$. The particle energy ranged from 0.6 up to 120 keV, which involves that for heavier particles the energy loss caused by the elastic scattering (nuclear stopping) dominates over the inelastic energy losses (electronic stopping). A definition of the different stopping parameters and an analysis of the possible systematic errors caused by the multiple scattering are given. The results of the measurements are compared with the theory of LINDHARD, SCHARFF and SCHIØTT.

Printed in Denmark
Bianco Lunos Bogtrykkeri A/S
ISBN 87 7304 034 7

1. Introduction

Even though the penetration of atomic particles into matter now has been studied for about half a century, further experimental investigations are strongly needed in the low energy part of the range in which the energy loss due to the elastic scattering equals or exceeds the inelastic energy losses.

The stopping due to the elastic scattering (in most literature called the nuclear stopping) was discussed by BOHR[1] in 1948. The BOHR theory was further developed by LINDHARD and SCHARFF[2] and by LINDHARD, SCHARFF and SCHIØTT[3] (in the following referred to as L.S.S.). They derived a universal curve for the nuclear stopping power by using the Thomas-Fermi model of the atom to determine the screening effect from the electrons on the nuclear Coulomb interaction potential between the colliding particles. Also using the Thomas-Fermi model LINDHARD and SCHARFF[2] developed a theory for the inelastic losses (the electronic stopping power) and found these to be proportional to the particle velocity, over the energy range in which the nuclear stopping is of importance.

In figure 1 is shown the theoretical universal curve for the nuclear stopping power $(d\varepsilon/d\varrho)_n$ together with a typical electronic stopping power curve $(d\varepsilon/d\varrho)_e$ and the resulting total stopping power curve $(d\varepsilon/d\varrho)_t$. The particle energy E and the range R are replaced by the dimensionless parameters ε and ϱ as defined in L.S.S.[3].

Systematic measurements of the pure electronic stopping power at higher ε-values, ORMROD and DUCKWORTH[4], ORMROD et al.[5], HVELPLUND[6] and HÖGBERG[7], have shown rather strong oscillations around the theoretically predicted values due to atomic shell effects.

An experimental test of the theory of the nuclear stopping in the energy range below the crossing of the nuclear- and electronic stopping power curves, i.e. $\varepsilon < 4$, is desirable, but until now very few such measurements exist. In 1963, with a gas cell with two small openings followed by an electrostatic energy analyser, very heavy particles with ε-values from 0.01 to 1 was studied

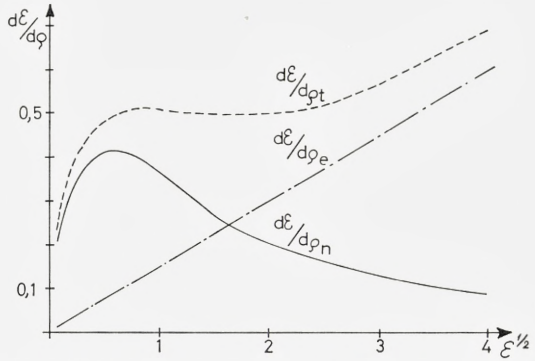

Fig. 1. Theoretical stopping power curves from LINDHARD, SCHARFF and SCHIØTT[3].

by SIDENIUS[8]. With time-of-flight method and α-recoils the stopping in thin solid films was measured by ZAHN[9] in 1963, MARX[10] in 1966, POOLE et al.[11] in 1967 and HANCOCK et al.[12] in 1969; the method is very limited in particle- and energy range, but allows measurements with ε-values about 0.1. In 1971 the stopping of $3 < Z_1 < 18$ ions with 4.5 to 46 keV energy (ε-values from 0.7 to 21) was measured in carbon foils by HÖGBERG[7, 13].

However, in all these measurements a narrow acceptance angle of the detection system was used. The measured stopping power is therefore what we shall call the stopping power in the forward direction, which in most cases differs from the total mean stopping power. It is therefore of importance to define as clearly as possible the various stopping data found from theory and experiment and to discuss the obtainable accuracy before the description of the present experiment.

2. Definition and Analysis of Stopping Parameters

The different parameters observable for a beam of particles penetrating a stopping layer will first be summarized. As stopping media only gases and amorphous solids are considered. The stopping layer shown in figure 2 is homogeneous matter with the molecular density N_m and plane parallel surfaces separated by the distance d. Ideally the matter consists only of atoms of one element with the atomic number Z_2 and the mass number M_2, but in practice compound molecules must also be considered.

The incident particle beam is considered to be ideal, i.e. a parallel, monoenergetic, narrow beam entering the stopping medium perpendicular to the surface. The incoming particles have atomic number Z_1, mass number

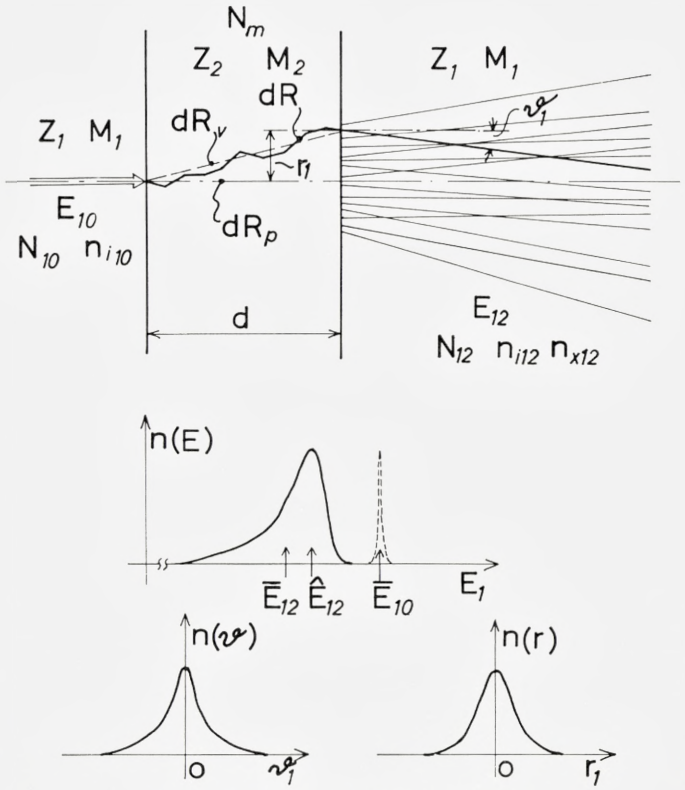

Fig. 2. Definition of stopping parameters.

M_1, and energy E_{10}, their number per unit time is N_{10}, and their charge state is n_{i10}.

The primary particles emerging from the stopping layer are well defined only in element and mass, Z_1 and M_1, and the number of particles leaving per unit time N_{12}, whereas the rest of the parameters are now described by distribution functions. In many cases these are non-Gaussian and non-symmetric, as shown in figure 2.

From the energy distribution $n(E_{12})$ one may derive, the mean energy $\bar{E}_{12}$, the most probable energy $\hat{E}_{12}$, and one or more parameters defining the shape of the distribution.

The multiple scattering, which is directly correlated to the nuclear stopping cross section, produces two phenomena: an angular deflection distribution $n(v_1)$ and a radial displacement distribution $n(r_1)$ in the emerging primary particles. As a rule, the radial displacement is measurable only

when the stopping element is a gas, whereas the angular deflection can be rather easily measured for a solid stopping element, but only with difficulty when the stopping element is gaseous.

Important information is contained in the relative abundances of the charges, n_{i12} and excited states, n_{x12} of the emerging primary particles. The study of these effects using beam foil spectroscopy[14] and beam gas spectroscopy[14] has become a growing field in the last few years.

Not shown in figure 2 is the secondary particle emission; from both the front and rear surfaces recoil target atoms and electrons will be ejected. These will be widely distributed in energy, angle, charge state, relative abundance, etc.

Important information about the slowing down process is contained in the ionization and excitation of the target atoms, effects which normally are observable only in a gaseous stopping element. For the present experimental technique the number of ionpairs created in the stopping layer per penetrating particle, dN_i, as well as the total number of ionpairs N_i created along the whole range of the particle are especially important parameters.

Figure 2 also illustrates the definition of the different stopping lengths. dR is the actual path length, dR_v is the vector length defined as the linear distance between the entrance- and exit points of the particles, and dR_p is the projected length as measured in the initial direction. For a plane parellel layer dR_p is the same as the thickness d.

In the L.S.S. theory[3] the stopping power is defined as the average energy loss dE per unit path length dR.

$$(dE/dR)_{th} = N_2 S = N_2 \int T d\sigma(T) \tag{1}$$

where N_2 is the number of scattering centers per unit volume and S is the stopping cross section per scattering center. This is not a real cross section, but is the average energy loss per scattering center. $d\sigma(T)$ is the differential cross section for the energy transfer T, which may be both elastic and inelastic. Normally it is impossible to observe the path length dR; therefore, to define the experimental stopping power, either dR_v or dR_p will have to be used. dR_p is the only stopping length, which can be measured for both a solid and a gaseous stopping layer. Hence the fundamental experimental stopping power is defined as

$$(dE/dR)_{tm} = \frac{dE_{tm}}{dR_p} \frac{E_{10} - \bar{E}_{12}}{dR_p} = \frac{E_{10} - \frac{1}{N_{12}} \sum_0^{N_{12}} E_{12}}{dR_p}. \tag{2}$$

This is the *total* mean stopping power, i.e. the energy analysis shall include all emerging primary particles, independent of their angle, radial displacement and charge state*.

If the energy analysis excludes some of the emerging primary particles, as hitherto always has been the case, a *fractional* mean stopping power is obtained

$$(dE/dR)_{fm} = \frac{dE_{fm}}{dR_p} = \frac{E_{10} - \frac{1}{N_f}\sum_0^{N_f} E_{12}}{Rd_p}. \qquad (3)$$

The most common fractionization is the exclusion in the energy analysis of all charge states except singly charged ions. If the stopping layer is much thicker than is needed to ensure charge equilibrium the charge fractionization should not be expected to introduce any significant error, even though ALLISON[15] has shown that there is a pronounced difference in the electronic stopping of neutral, singly or doubly charged particles.

In the case of a solid stopping layer a rather common fractionization is the exclusion of emerging particles with an angular deflection larger than a normally very small angle θ_{ac} determined by the acceptance angle of the energy analyser.

For a gaseous stopping layer the use of a small outlet opening excludes emerging particles with a radial displacement larger than the opening radius r_0; often a further exclusion follows due to the limited acceptance angle of the energy analyser. Here, it may be worthwhile to note that when M_1/M_2 is close to unity about 30 % of the nuclear stopping is caused by collisions with a deflection of the primary particle larger than 45 degrees!

If the measurement is performed in the forward direction with a small acceptance angle the measured energy loss is caused mostly by the electronic stopping. This has been utilized in measurements of the pure electronic stopping[4, 5, 6, 7]. However, for a test of the nuclear stopping theory it is an absolute requirement that the energy analysis incorporates all emerging primary particles. Only for very heavy particles stopped in a light gas ($M_1/M_2 > 100$) and a thick stopping layer is the fractionization effect negligible[8]. HÖGBERG[7, 13] has studied the influence of the target thickness and used it to determine what he calls the saturation value of the nuclear stopping, but it still is the stopping in the forward direction and all large angle scattered particles are excluded.

* More correctly, the last term should be $\frac{1}{N_{10}}\sum_0^{N_{12}} E_{12}$, since particles may be stopped completely in the layer.

Since dR_v is more closely related to the path length dR than is dR_p, a better test of the theoretically predicted stopping power would be obtained by a measurement of the total mean vector stopping power:

$$(dE/dR)_{tmv} = \frac{dE_{mv}}{dR_v} = \frac{E_{10} - \frac{1}{N_{12}} \sum_0^{N_{12}} E_{12}}{dR_v}. \tag{4}$$

(4) is the same as (2) except that dR_v replaces dR_p, i.e. instead of a plane exit surface a sperical surface with the radius dR_v is used.

In practice such measurements are possible only in a gas and only by using an outlet opening, which can be rotated around the inlet opening, thus permitting integration over all angles. A few unpublished measurements of this kind using a slight modification of the equipment described in ref.[8], confirmed the previously measured stopping power data for $^{69}_{31}$Ga in H_2 gas except for a correction factor of 1.1. However, the measurements still suffered from a limited acceptance angle of the energy analyser.

A search for an energy analyser for low energy heavy particles with a fractionization effect as small as possible was initiated; the resulting heavy ion detector is described in section 4. It permits measurements with very low energy particles and it has solved nearly all problems connected with the fractionization effects. It is, however, sensitive also to the recoils and their influence is therefore discussed in the following section.

3. The Recoil Effect

For $M_1 = M_2$ a maximum energy (T_m) equal to the total energy E_1 of the primary particle may be transferred to the secondary particle in a single collision. Since secondary and primary particles are indistinguishable, a fundamental and serious experimental problem is created. As a result of the rather slow variation of T_m with M_1/M_2, the problem is present for a wide M_1/M_2 range.

Theoretically, it will be so, that if a very thin stopping layer with approximately single collision condition is placed in front of a detector with a 2π acceptance angle and the electronic stopping is negligible, all the recoil energy will be transferred to the detector. If the detector then linearly sums the energies of the primary particle and its accompanying recoil particles, the result will be a 100 $^0/_0$ error in the measurement of the elastic energy loss!

This is, however, for an ideal linear detector which gives a voltage signal proportional to the particle energy E_p. Fortunately the detector used in the present experiment is not ideal and the signal is a nonlinear function of the heavy particle energy. This, as will be shown, helps to decrease the error of 100 % to less than 33 %.

The detector is a low pressure proportional counter which gives a signal proportional to the number N_i of ion pairs formed in it by the particle. N_i, however, is not proportional to the energy E_p of the particle, but (see part 7 and figures 6 and 7) empirically N_i was found to be approximately

$$N_i = \frac{E_p}{W_i} \simeq \frac{E_p}{\frac{k_1}{k_2 E_p} + k_1} \tag{5}$$

W_i is the average energy needed to create an ion pair, which for low particle energy will be

$$W_i \sim \frac{k_w}{E_p} \tag{6}$$

and hence

$$N_i \sim \frac{E_p^2}{k_w}. \tag{7}$$

The detector is followed by an electronic analog device, which makes the output U_d proportional to the particle energy

$$U_d = \sqrt{\frac{A_t}{k_w} E_p^2} = k_d E_p \tag{8}$$

A_t is the total gain of the system and k_1, k_2, k_w, k_d are constants.

Suppose $M_1 = M_2$ and hence $T_m = E_1$. With no stopping layer the signal U_{d0} is

$$U_{d0} = k_d E_{10}. \tag{9}$$

With a stopping layer inserted and assuming the recoil atoms *not* to reach the detector, the signal corresponding to an energy transfer T is

$$U_{d1} = \sqrt{\frac{A_t}{k_w} (E_{10} - T)^2} = k_d (E_{10} - T) \tag{10}$$

whereas if the recoil atom reaches the detector, the signal is, k_w here being the same for particle and recoil atoms:

$$U_{d2} = \sqrt{\frac{A_t}{k_w}((E_{10} - T)^2 + T^2)} = k_d\sqrt{(E_{10}^2 - 2T)^2 + T^2}. \tag{11}$$

The difference between U_{d0} and U_{d1} is correctly proportional to the energy loss T

$$u_1(T) = U_{d0} - U_{d1} = k_d T \tag{12}$$

whereas the difference between U_{d0} and U_{d2} is

$$u_2(T) = U_{d0} - U_{d2} = k_d(E_{10} - \sqrt{E_{10}^2 + 2T^2 - 2E_{10}T}) \tag{13}$$

which may be written, introducing the ratio r_T:

$$r_T = \frac{T}{E_{10}} \tag{14}$$

$$u_2(T, r_T) = k_d T\frac{1 - \sqrt{1 - 2r_T + 2r_T^2}}{r_T} = u_1(T)f(r_T). \tag{15}$$

The function $f(r_T)$ is shown in figure 3 together with the relative error

$$\Delta u(T)/u_1(T) = \frac{u_1(T) - u_2(T)}{u_1(T)}. \tag{16}$$

As seen the relative error is nearly proportional to T.

Next we want to find the average energy loss, dE_n, and its error. We use the simple power law cross section from L.S.S.[3] with $s = 2$, and obtain, introducing the ratio r_T,

$$d\sigma(r_T) = \frac{C_2}{E_{10}r_T^{3/2}}dr_T \tag{17}$$

where the constant C_2 is equal to half the value of the nuclear stopping cross section, which is independent of energy.

The average voltage signal $\bar{u}_1$ for the correct measurement will be

$$\bar{u}_1 = k_d\, dR N_2 \int_0^1 E_{10} r_T \frac{C_2}{E_{10}r_T^{3/2}}dr_T = k_d\, dE_n. \tag{18}$$

According to fig. 3 $u_2(T, r_T)$ may be approximated by $u_2 = k_d E_{10} r_T (1 - r_T)$, and the average signal obtained, if recoils reach the detector, is

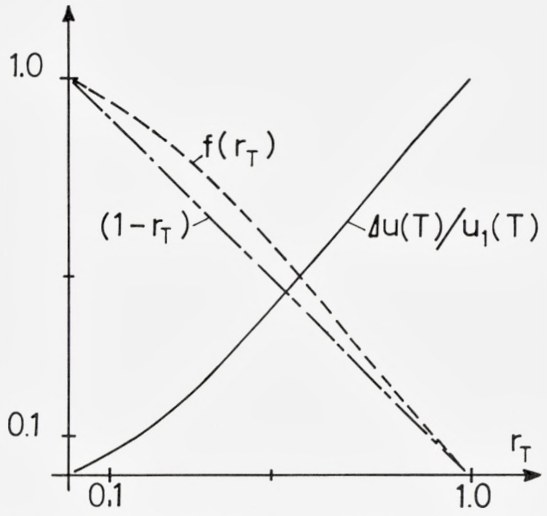

Fig. 3. The recoil influence in single collision events plotted as a function of $r_T = T/E_{10}$. The function $f(r_T) = u_2/u_1$ is the ratio between the recoil influenced signal and the correct signal and $\Delta u(T)/u_1(T)$ is the relative error.

$$\bar{u}_2 = k_d dR N_2 \int_0^1 E_{10} r_T (1 - r_T) \frac{C_2}{E_{10} r_T^{3/2}} dr_T = \tfrac{2}{3} k_d dE_n . \tag{19}$$

When M_1/M_2 deviates from unity, the difference $\bar{u}_1 - \bar{u}_2$ is smaller and thus the relative error in the energy loss measurement never exceeds 33 %.

This is for an assumed single collision condition, where the energy distribution of the recoils is proportional to $r_T^{-3/2}$ but in an actual stopping layer with multiple collision condition the energy distribution is expected to be proportional to r_T^{-2} as has for instance been found for sputtered particles[16]. With such a distribution the relative error is reduced to less than 20 % and the angular scattering and inelastic losses will further reduce this value.

This was demonstrated by a calculation of the fraction of the total elastic energy loss, which reaches the detector volume as recoil energy. As above, the power law cross section with $s = 2$ and $M_1 = M_2$ was used, and it was assumed that the stopping consists of a part independent of energy, called the homogenenous part, caused by inelastic stopping and small angle collisions and a part caused by large angle collisions.

The results are shown in figure 4. The thickness ΔR of the stopping layer was varied, and the ratio r_E between the homogeneous energy loss in ΔR and the primary particle energy E_1, is used as a parameter. dE_n is the

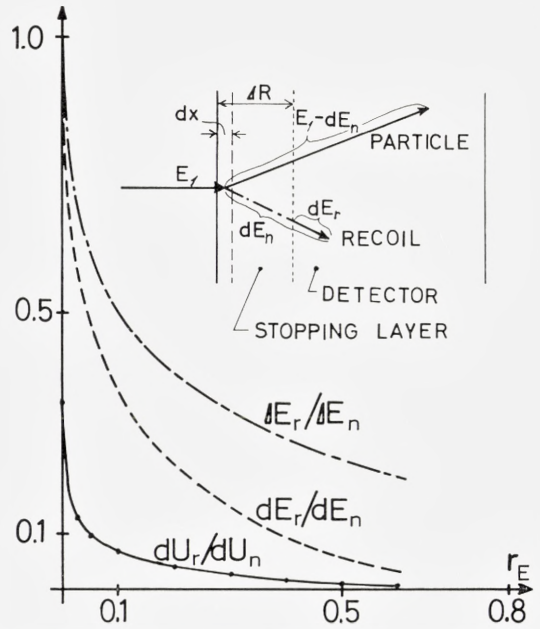

Fig. 4. Fraction of the elastic energy loss transported by recoils into the detector from dx, (dE_r/dE_n), and from ΔR, ($\Delta E_r/\Delta E_n$) and the relative error, dU_r/dU_n, on the detector signal plotted as functions of the parameter r_E (see text). A single event is shown very schematically.

total elastic energy loss in a thin layer dx next to the entrance surface. dE_r is the part of dE_n which is transported through the stopping layer ΔR to the detector. ΔE_r and ΔE_n corresponds to the whole stopping layer.

Especially dE_r/dE_n is strongly affected by the total stopping layer thickness. This leads to the conclusion that the best method in stopping power measurements is to add stopping layers in increments of dx, adjust the primary particle energy for each step with an energy increment dE so that the average detector signal stays constant and in this way obtain a dE/dx value. Hereby it is obtained, that in the layer between the dx layer and the detector volume the particle energy and the recoil balance is nearly unchanged and the error is caused only by the recoils from dx and hence, as seen from figure 4, decreases rapidly with increasing thickness of the total stopping layer.

If the reduction effect of the detector nonliniarity is also taken into consideration, the resulting relative error on the detector signal, dU_r/dU_n, shown in figure 4 is obtained. Thus the error is very small, except for the first few steps in a measurement.

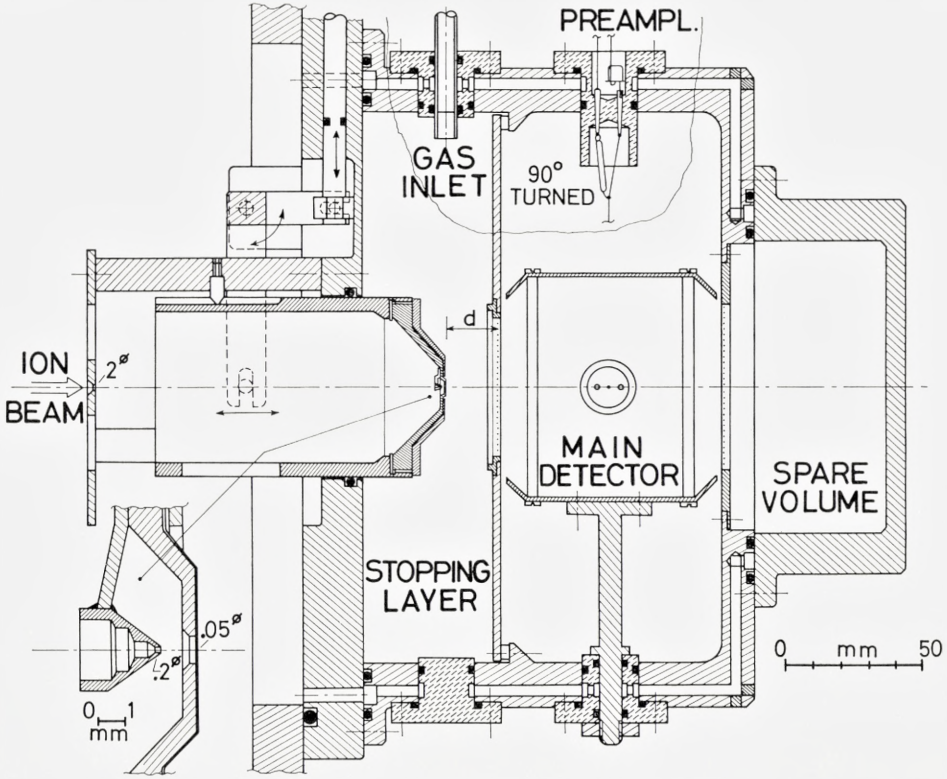

Fig. 5. The mechanical design of the detector system.

4. Experimental Apparatus

The fundamental problem of obtaining full transmission from the stopping layer to the energy analyser is solved by using a low pressure proportional counter as the energy detector and through the use of the same gas in the stopping layer and in the detector thus permitting the use of a high transmission grid between them.

In figure 5 is shown a somewhat simplified drawing of the system. The ion beam which is precollimated by a 2 mm diameter aperture enters the gas through a 0.05 mm diameter opening in a 0.05 mm thick stainless steel foil.

When a gas target is used, the beam inlet opening presents a problem, because of the difficulty in defining the exact boundary between the vacuum

and the gas. With the present small opening, the vacuum in the accelerator is hardly affected. The gas molecules are therefore streaming out with a mean free path of the order of many centimeters and a density which drops off with distance so fast that the addition to the gas layer caused by the outstreaming gas, when converted to the pressure inside the chamber, is smaller than the diameter of the opening, and therefore negligible.

Since the ion beam outside the opening easily contains up to 10^6 times more particles than the number, which enters the chamber (normally about 10^3 per second), the scattering in the outstreaming gas is not negligible. An antiscatter aperture, shown in fig. 5 in larger scale, reduces the number of scattered primary particles and recoil atoms, which otherwise would give rise to a low energy background in the detector, to a nearly nondetectable level.

The beam inlet opening is placed on a cylinder movable along the axial direction, so that the distance d to the grid can be varied, from zero to 40 mm. d is measured with a micrometer to an accuracy of $\pm$ 0.02 mm. By means of a linear potentiometer mechanically connected to the cylinder an electric signal indicating the position is obtained. The cylinder is insulated to allow the use of a bias voltage.

The central wire in the detector is a 0.11 mm diameter W-wire; the outer detector walls are 80 mm apart and have a length of 200 mm. By means of an α-source with a 3° collimation, the electron collection efficiency and the gas amplification were tested and found to be constant to better than 1 % over the whole volume where ion pairs are formed by the primary particles.

The entrance opening to the detector has a diameter of 50 mm and is covered by a grid, formed by 0.05 mm diameter N_i-wires spaced 0.5 mm.

To minimize disturbing effects from ionization of impurity atoms by metastable states of the detector gas atoms (Penning effect) the highest purity of the gas is essential. Double O-ring seals were used everywhere in the apparatus and in the gas inlet system. The volume between any pair of O-rings was connected to high vacuum and thus no impurities could leak into the gas, which was taken from high pressure bottles with an impurity content less than 0.01 %. The gas pressure, which ranged from 3 to 15 Torr, is stabilized to better than 1 part in 10^3 over periods of several hours by a special oilmanometer system[17] with both optical and electrical read-out of the oil level, and an electronically controlled leak valve[18]. The system is held at 22° C $\pm$ 0°.1 C.

The detector electronic system is standard equipment for pulsehandling except for two special modules. One is the inlet control box, which ensures that there is the same field strenght but in opposite directions on the two

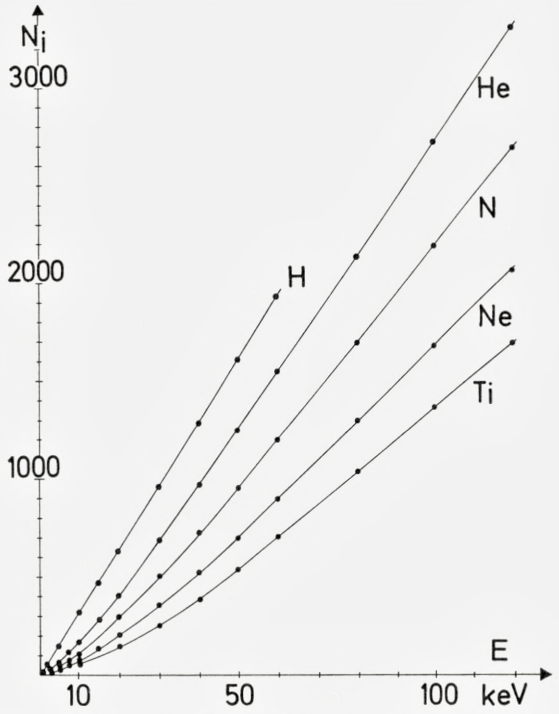

Fig. 6. Number of ion pairs formed in Methane by five different particles plotted as functions of the particle energy.

sides of the entrance grid of the detector for all positions of the inlet system, wherefore electrons formed outside the detector volume are not collected on the detector wire.

A 512 channel pulse height analyser is used to analyse the pulse height distributions. But since the energy distribution often is unsymmetric, and since a quick determination of the mean energy is essential, a special electronic unit, the C.M.C.[19], was designed and connected to the pulse height analyser. It permits a calculation of the center of mass channel number to be made in less than 10 seconds and displayed on a scaler with an accuracy of 0.1 channel.

5. The Energy Detector

With CH_4 as the detector gas the number of ion pairs N_i as a function of the particle energy E was investigated in the energy range 10–120 keV for particles with $Z_1 \leq 22$ by Macdonald and Sidenius[20]. Figure 6 shows some

typical examples of $N_i = f(E)$ curves. Figure 7 gives the N_i dependency on Z_1 for fixed energies and, as seen, the oscillations found in the measurements of the pure electronic stopping[4, 5, 6, 7] also show up here.

This complex relation between N_i, E, Z_1, which itself gives important information about the slowing down of low energy heavy particles, involves that, for the proper use, the detector must be calibrated for each particle-gas combination.

As seen in figure 7, the number of ion pairs formed by the very low energy heavy particles is of the order of 10 to 100 and consequently the resolution of the detector is primarily determined by the statistical fluctuations in these low numbers. At higher energies, the fluctuations in the different energy loss processes will set the limit in resolution. The best resolution obtained has been about 5 % F.W.H.M. for 50 keV H^+ in CH_4.

The electronic noise from the preamplifier is almost without influence on the resolution, but sets the limit for the lowest energy, which can be detected. To allow the detector to work with the lowest gas amplification, which gives the most stable condition, a low noise preamplifier with a F.W.H.M. noise of about 250 ion pairs is used. With a gas amplification of about 200 the pulse height distributions from a mean value of 10 primary ion pairs are completely resolved from the noise.

With CH_4 as detector gas the gain stability is better than 0.2 % for several hours, whereas other gases require the use of a gain stabilizer to give the same stability.

6. Measuring Methods and Procedure

Two methods of stopping measurements are possible. In the variable pulse height method (V.P.H.) the incident particle energy E_{10} is kept constant and the shift in the average energy E_{12} of the emerging particles is observed as a function of the stopping layer thickness d. In the constant pulse height method (C.P.H.) the incident particle energy E_{10} is adjusted as a function of the stopping layer d so that the average energy E_{12} of the emerging particles is kept constant.

In principle the two methods should yield the same results, but they differ in their sensitivity to the multiple scattering effects, the V.P.H. method being the more sensitive. Furthermore, the data analysis is much more difficult for the V.P.H. method because the pulse height data must be converted into energy data via the calibration curve; this introduces unnecessary errors. The V.P.H. method was therefore disregarded except for a few

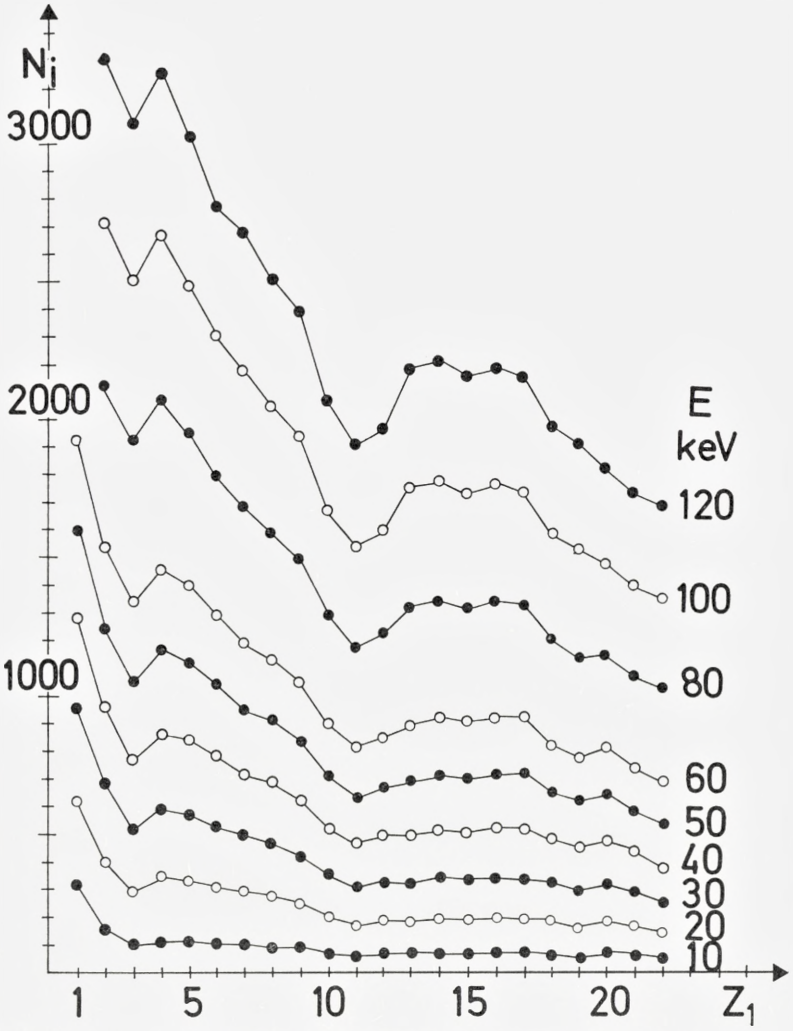

Fig. 7. Number of ion pairs formed in Methane plotted as functions of the atomic number Z_1 of the incoming particle and with the energy as parameter.

measurements with protons for which the calibration curve is linear and for which the V.P.H. method can be used to a somewhat lower energy than can the C.P.H. method.

The particles are produced by the reconstructed, 30 year old Copenhagen isotope separator[21]; now used as a modern universal range ion accelerator and separator (URIAS)[22]. The ions are mass analysed at a fixed energy

and afterwards either retarded or post accelerated. Thereby it is possible to obtain singly charged particles of continuously variable energy from less than 1 keV up to 60 keV. For higher energies doubly or triply charged ions are used.

The ions are produced in a high temperature universal ion source[23] with an energy spread of less than than one electron volt. The energy of the ions is measured with a digital voltmeter to an accuracy of $\pm$ 0.1 %.

After a suitable target gas pressure is set with $d = 0$, the particle energy is set to the lowest value E_{10}, and the center of mass value N_{CM0} for the impulse height distribution is found using the C.M.C. The inlet system is then displaced one millimeter and the particle energy adjusted until N_{CM1} read approximately the same as N_{CM0}, and both d, E_{11} and N_{CM1} are recorded.

This procedure is repeated for increasing distances until the E_{12} distribution becomes so broad that the low energy tail extends down to the noise. d is then turned back to zero and the stability of the system checked through the measurement of N_{CM0} at energy E_{10}.

A new value of E_{10} is then chosen, well inside the energy range covered in the first run, and the measurements are repeated.

The E_1 data are corrected for the small difference between N_{CM0} and N_{CMn}

$$E'_{1n} = E_{1n} + E_{10}\left(1 - \frac{N_{CMn}}{N_{CM0}}\right) \tag{20}$$

the dE/dx for each 1 mm step increment is found as

$$dE/dx = \frac{E'_{1\,(n+1)} - E'_{1n}}{dx} \tag{21}$$

and the data are normalized for different pressures etc. by converting them into the molecular stopping cross section S_x, the average energy loss per stopping molecule.

The statistical fluctuations in S_x from these small values of dx and dE is normally rather large, up to $\pm$ 10 %, but they are useful for an estimate of the quality of the measurements. Another test of the quality of the measurements is obtained by the requirement that the various (E'_1, d) curves corresponding to different E_{10} starting values must accurately fit together to form a smooth curve. Figure 8 shows, as an example, curves for Nitrogen stopped in Methane. Not all the single curves used to obtain the final curve are shown. The points from the different measurements are scattered less than 1 % in the

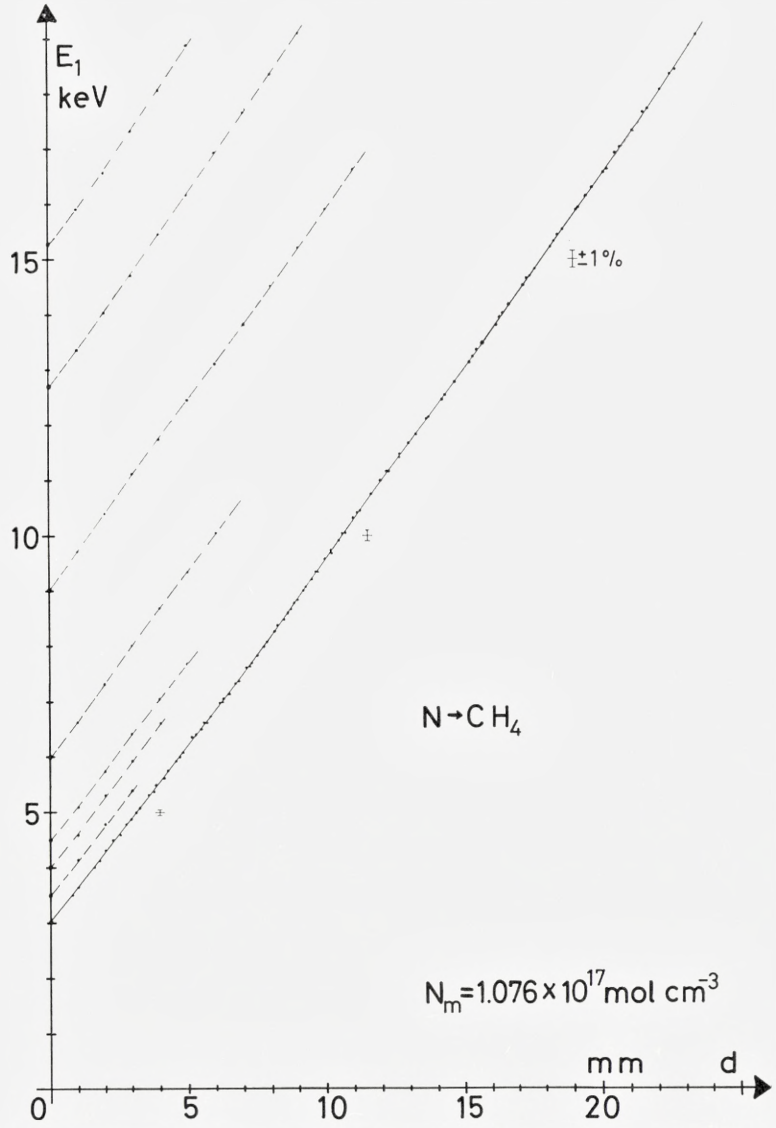

Fig. 8. Primary energy, E_1', plotted as function of distance, d, for constant mean energy after the stopping layer. The curves corresponding to different starting values (dotted lines) are fitted together to form the final energy-range curve (full line) for Nitrogen stopped in Methane.

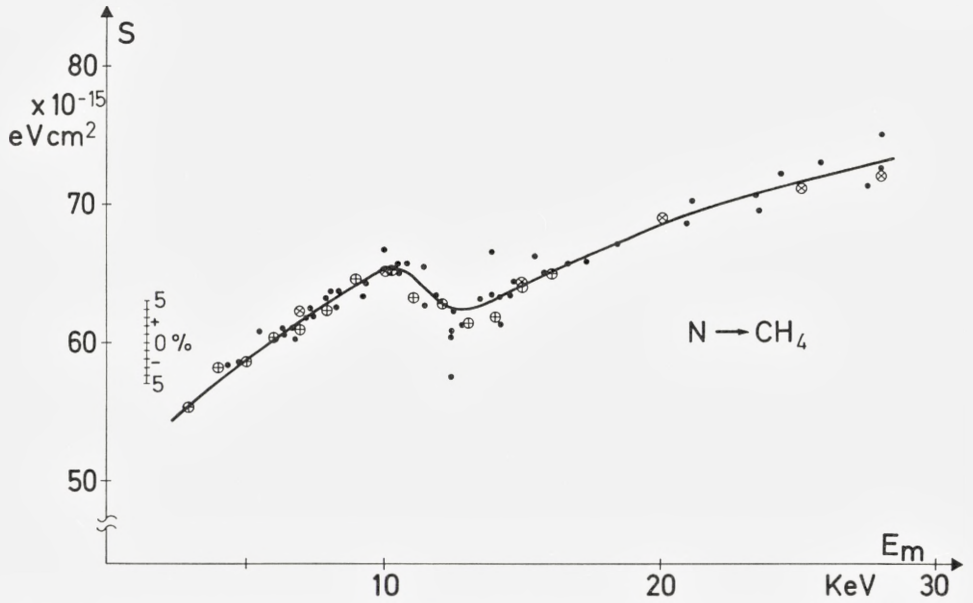

Fig. 9. Low energy part of the stopping cross section curve for Nitrogen stopped in Methane. Points are from the data analysis described in the text, crosses are from a differentiation of the final curve in figure 8.

low energy range and less than $^1/_2$ % in the high energy range. Points from two sets of measurements with pressures of 3.20 and 6.40 Torr are shown.

Figure 9 shows the low energy part of the stopping cross section curve for Nitrogen slowed down in CH_4. A rather narrow structure, at approximately 10 keV, is seen. The points are from the data analysis described, but using values of dx from 3 to 6 mm, and the average spread around the smooth curve is about $\pm$ 2.5 %. As a comparison a differentiation of the final energy-range curve in figure 8 yielded results shown as circled crosses; there is satisfactory agreement between the results found by the two different analysing methods.

7. Systematic and Statistical Errors

In the C.P.H. method a calibration curve is, in principle, not needed, but due to the nonlinear pulse height-energy relation a systematic error is introduced. With increasing stopping layer thickness the energy distribution becomes wider due to the straggling and if two distribution curves having the same center of mass but different widths are each folded with the same non-

linear function the resulting curves will not have the same center of mass. Therefore to the main pulse height amplifier was added a variable nonlinear stage, which served to straighten the pulse height-energy curve to a linear curve without any loss in the overall stability.

As previously shown, a systematic error arises from recoils reaching the main detector. However, the detector reduction effect and the use of the C.P.H. method reduce this error to less than 5 to 10 % of the elastic stopping except for the first one or two mm stopping layer.

Any possible systematic error will be strongly dependent on the stopping layer thickness. The best estimate of their influence is obtained by measurements of dE/dR data for the same mean energy but measured with different layer thicknesses and at different distances from the grid.

As shown in figure 8 and 9, except for the first one or two mm of stopping layer such differences in stopping data were found to be smaller than the statistical uncertainties. For the present measurements in CH_4, it is estimated that in the region from 3 to 10 keV the systematic error is less than -5 to $+15$ %, from 10 to 30 keV less than -3 to $+10$ %, and from 30 up to 120 keV less than -2 to $+4$ %.

The statistical fluctuation in the mean value of the E_{12} distribution varies from ± 0.5 % at low energies to ± 0.2 % at high energies. Since dE is determined as the difference between two nearly equal numbers, (dE is normally less than 10 % of E_{12} except at low energies) the fluctuation in dE and therefore in the stopping power ranges from ± 2.5 % to ± 7 % depending on the magnitude of dE and E_{12}.

All the present stopping cross section curves are results of many repeated measurements carried out with different pressures.

8. Results and Discussion

There are several reasons for choosing the most simple hydrocarbon, CH_4, as stopping gas. Firstly it is found to give optimum stability of the detector, secondly the content of the light H-atoms decreases the scattering and recoil effects, and finally the slowing-down of particles in hydrocarbons has great interest for the application of the stopping data in health physics and radiation damage theory, J. A. Dennis[24, 25].

As particles the first ten elements in the periodic system were used. The energy ranged from 0.6 keV up to 110 keV.

The data obtained are the total mean stopping power for the projected path given by formula (2) and they are not directly comparable with the

theory, which refers to the mean stopping along the actual path, as given by formula (1). Since no theoretical calculation of the total mean stopping for the projected path is available, no attempt was made to correct neither the experimental nor the theoretical data. But a correction of the theoretical curve would in all cases have resulted in an increase in the stopping cross section especially at low energy. Still, the theoretical curves, calculated from L.S.S.[3], will be of interest for comparison and they are therefore in all cases shown together with the experimental results.

For protons the stopping cross section curve from 0.6 up to 60 keV is shown in figure 10, together with other experimental results and the theoretical curve which is only valid up to about 15 keV. The agreement between the present results and those of Reynolds et al.[26] and Park and Zimmerman[27] is excellent, whereas a systematic disagreement exists with the measurements of Hughes[28]. The explanation seems to be that Hughes has used an ion source giving a high output of H_2^+ instead of H^+ and he has not used an analysing magnet. Much better agreement would be obtained if his energy scale was divided by two!

The stopping cross section for Helium ions was measured in the energy interval from 3 to 60 keV and is shown in figure 10. The theoretical curves for Helium and for the heavier particles to be discussed later were calculated as the sum of the nuclear and electronic stopping cross sections of the Carbon atom and the four Hydrogen atoms.

$$S_t = S_{nC} + S_{eC} + 4S_{nH} + 4S_{eH}. \tag{22}$$

The agreement between the present results and the theory and the results of J. T. Park[29] could have been better, but at least the slope is about the same. Park has used a very small analyser acceptance angle and this may be the reason for the discrepancy between the two experimental results.

At low energies, two interesting effects are observed. One is the bump in the curve at about 10 keV which seems to indicate some kind of resonance effect in the losses. Secondly, in disagreement with theory, the experimental curve does not level out below 5 keV.

That the latter is not a result of a systematic error is proved by the fact that no such effect is found for the two Lithium isotopes, as shown in figure 11. The agreement with the point of Teplova et al.[30] is reasonably good. The magnitudes of the experimental and theoretical values differ strongly, but this may be explained by difference in the electronic stopping. More important, the general behaviour of the two sets of curves is the same; note especially the crossing caused by the isotope effect.

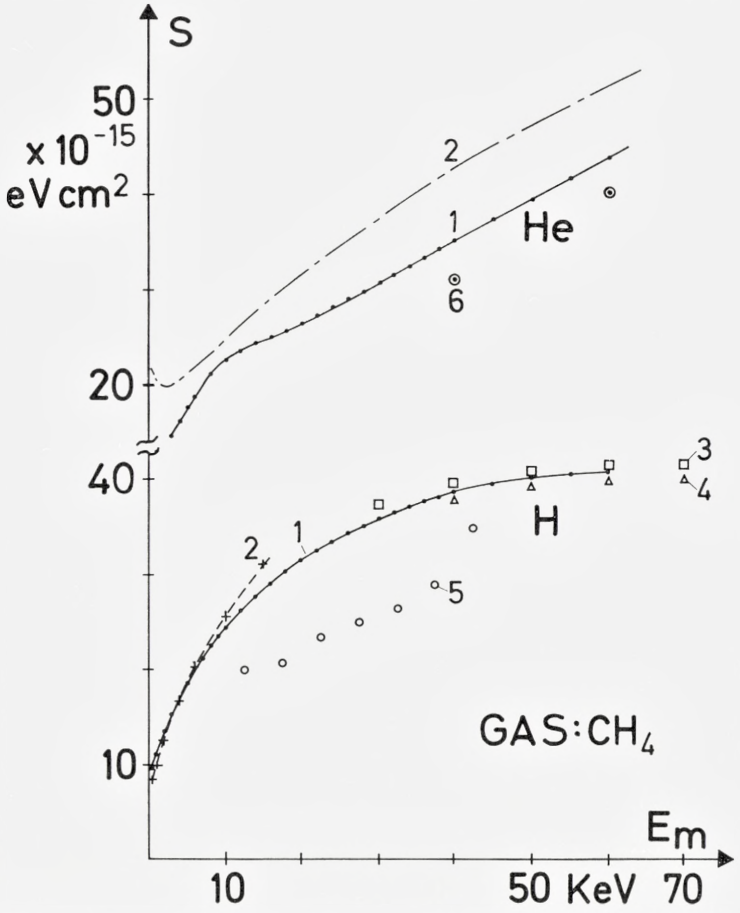

Fig. 10. Stopping cross sections for Hydrogen and Helium stopped in Methane. The curves marked 1 give the results of the present experimental investigations whereas 2 are the theoretical estimates. Other experimental results are: 3, REYNOLDS et al.[26], 4, PARK and ZIMMERMANN[27], 5, S. HUGHES[28], and 6, J. T. PARK[29].

Results for particles ranging from Beryllium to Neon are shown in figure 12 and 13. For all the particles the experimental stopping cross section at low energy is much lower than the theoretically predicted. A most striking feature is the pronounced structure in the curves for Nitrogen and for Carbon. If this structure is caused by the nuclear stopping one should expect a similar structure to appear for the neighbouring elements more pronounced than is the case; therefore the electronic stopping must be responsible for the structure. The broader structure of the Fluorine and the Neon curves rather seems to belong to the same type as the Helium curve.

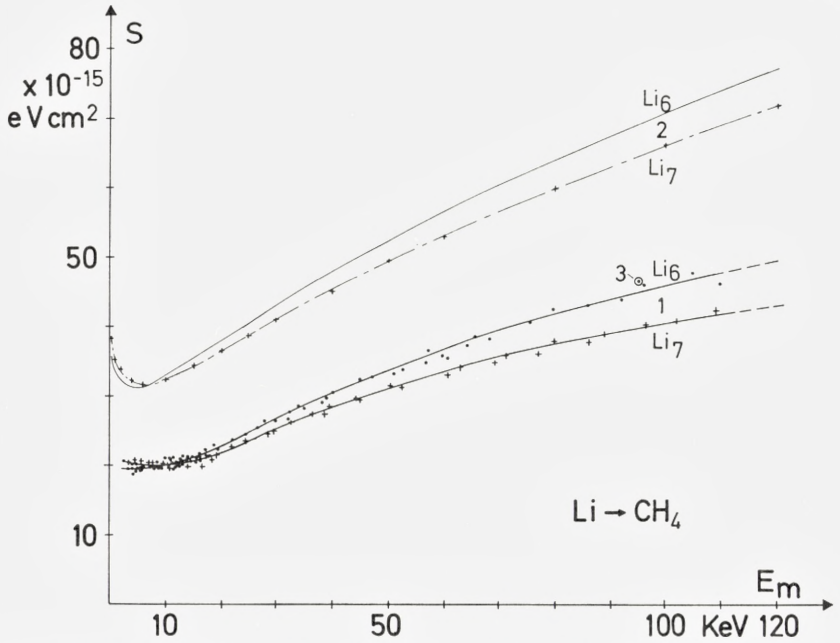

Fig. 11. Stopping cross sections for the two Lithium isotopes stopped in Methane. Curve set 1 gives the results of the present experiments whereas curve set 2 represents the theory. Point 3 is the experimental result by TEPLOVA et al.[30].

The agreement with the data of TEPLOVA et al. for Boron could have been better, whereas for Nitrogen there is surprisingly good agreement with the data of HUGHES, though these might have been expected, like for hydrogen, to be in error due to a dominating beam of doubly charged ions.

In figure 14 all the experimental results are shown together.

9. Deduction of the Electronic Stopping Cross Section

In the present investigations experimental values for the total stopping cross section were obtained. If we take the values for the various particles at a selected common velocity and subtract the corresponding theoretical values from L.S.S.[3] of the nuclear stopping cross section, values for the electronic stopping cross section Se may be obtained.

The resulting values of S_e for particles with the velocity $v = 0.5\ v_0 = 1.09 \cdot 10^8$ cm s^{-1} are plotted in figure 15 together with the theoretical estimates of S_e by L.S.S.[3]. Contrary to the smooth shape of the latter, the experimental values exhibit an oscillatory variation, for which the magnitudes of the

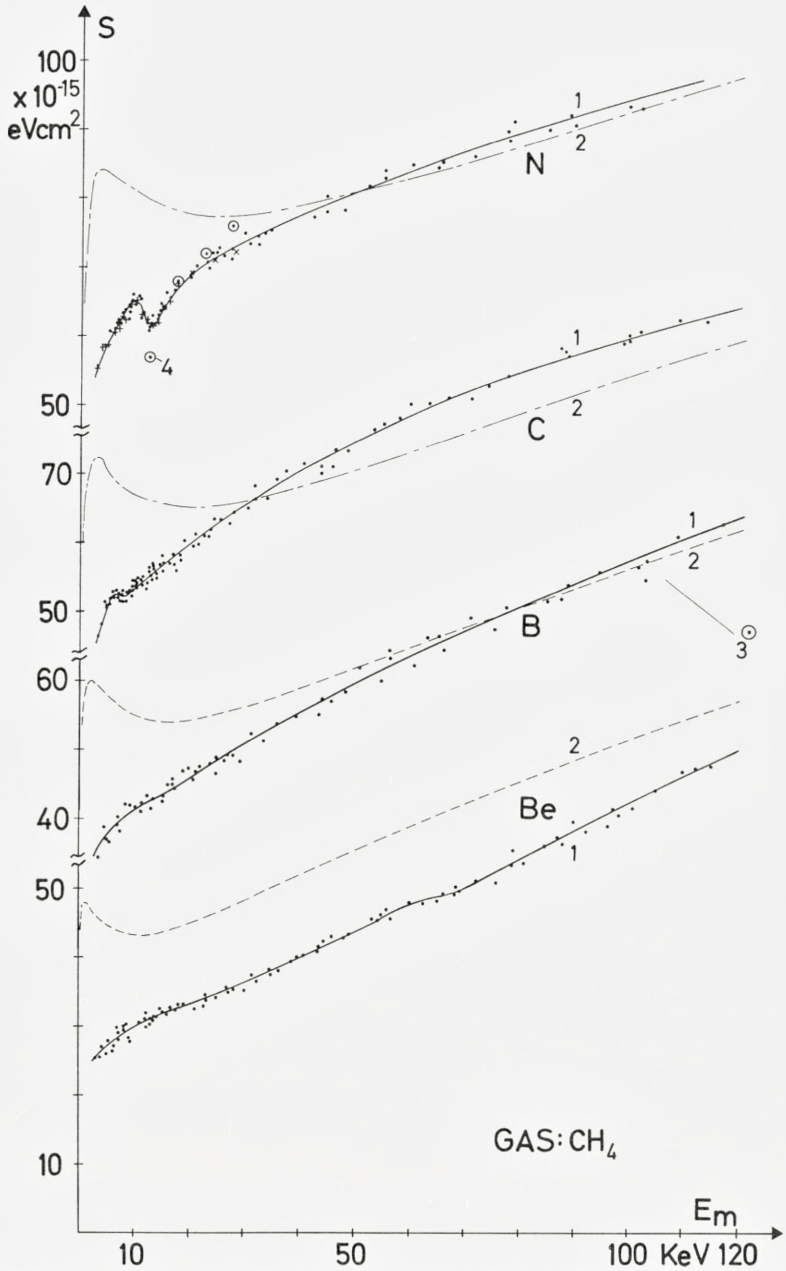

Fig. 12. Stopping cross sections for Berylium, Boron, Carbon and Nitrogen stopped in Methane. The curves marked 1 give the results of the present experiments, 2, are the theoretical estimates. Other experimental results are: 3, TEPLOVA et al.[30] and 4, S. HUGHES[28].

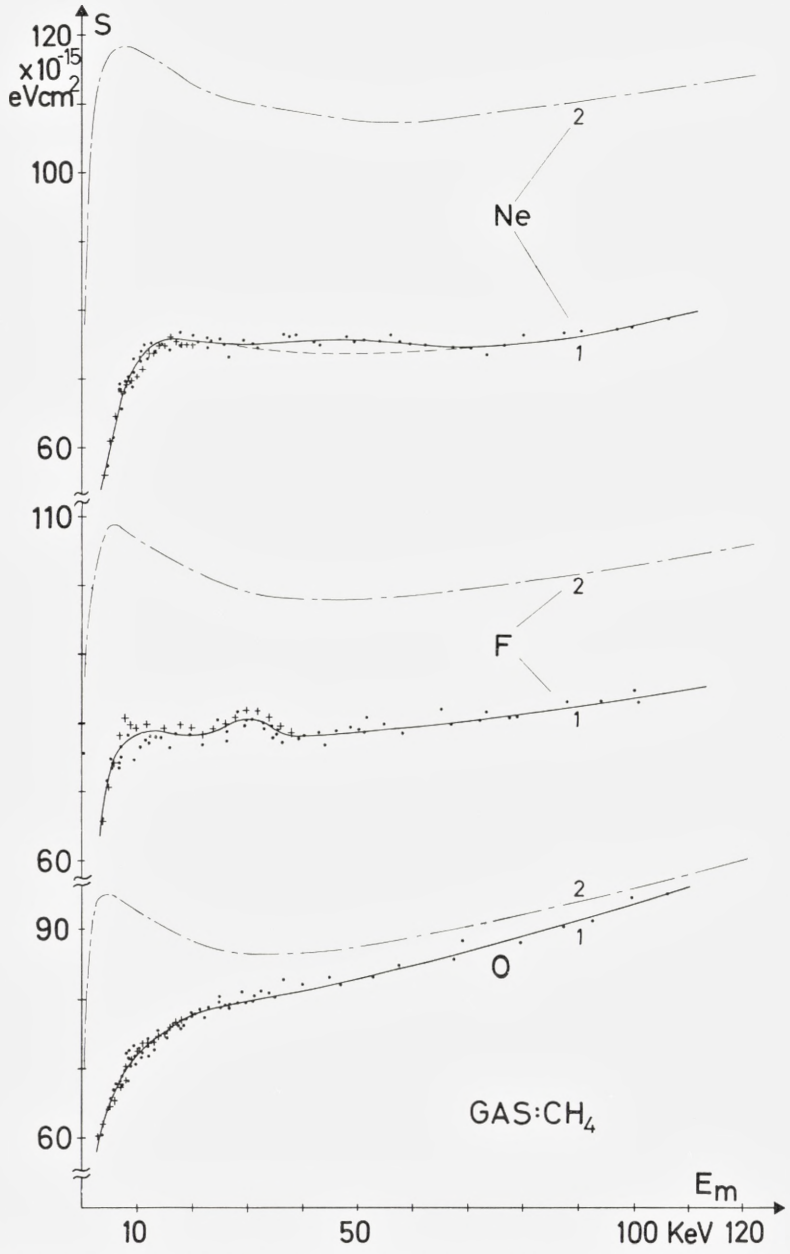

Fig. 13. Stopping cross sections for Oxygen, Fluorine and Neon stopped in Methane. The curves marked 1 give the results of the present experiments and 2 are the theoretical estimates.

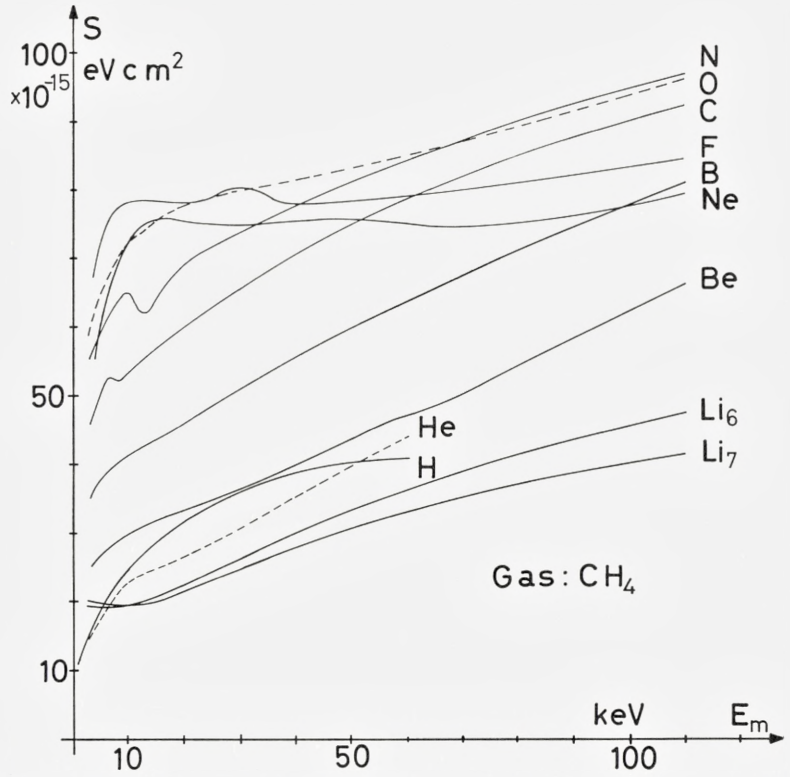

Fig. 14. Experimental total mean stopping cross sections for the first ten elements stopped in Methane.

maxima and minima are in good agreement with measurements in other gases by HVELPLUND[6].

At the selected velocity the theoretical nuclear stopping ranges, for the light particles from 10 % of the total experimental stopping up to 50 % for the heavy particles. Since the nuclear stopping seems to be overestimated by the theory (se next chapter) the deduced values for S_e are probably too low especially for the heavy particles. On the other hand the theoretical value refer to the actual path of the particle and the experimental value refer to the projected path, this causing the obtained values for S_e to be too high. The uncertainties in the values of S_e will therefore be of the order of $\pm$ 10 % for the light particles up to $\pm$ 30 % for the heavy particles.

10. The Nuclear Stopping Cross Section

The ultimate aim of the present experiment is to obtain information on the nuclear stopping. Since the nuclear stopping is most dominating in the stopping of the heavist particles, Neon shall be used as example in the following analysis. To learn about the nuclear stopping we might use the reverse of the procedure for deducing the electronic stopping, i.e. we might assume the theoretical value of the electronic stopping to be correct and subtract it from the experimental values of the total stopping. However since for Neon the experimental value of S_e in all measurements has been found to be much smaller than the theoretical estimate, the use of the latter without correction is not reasonable. Instead, two different values, S_{e1} and S_{e2} of the electronic stopping stopping cross section have been tried. S_{e1} is the theoretical value from L.S.S.[3], multiplied by the ratio between the present measured value and the theoretical value for the total stopping cross section at 120 keV. S_{e2} is the theoretical value multiplied by a factor obtained from measurements of the stopping of Neon in Air, HVELPLUND[6], and the stopping of Neon in Nitrogen, ORMROD[31]. Their measurements lead to almost the same ratio between the experimental and the theoretical values for the total stopping.

In figure 16 the resulting curves are shown. The choise between S_{e1} and S_{e2} is seen to be of importance for the experimental value of S_n at high energy, but rather unimportant for the position and magnitude of the maxima. Judging from the curves at high energies, where the slope of S_{n2} too quickly approaches zero, S_{e1} is a better choice than S_{e2}. The general shapes of the two curves S_{n1} and S_{nt} (curves 7 and 3) are in reasonable agreement, but the magnitudes and positions of the maxima differ.

Table 1 gives the ratios between the maximum values of the experimental and theoretical nuclear stopping cross sections, $r_{\hat{S}} = \hat{S}_{n1}/\hat{S}_{nt}$, and the ratios of the energies corresponding to these maxima, $r_{\hat{E}} = \hat{E}_{n1}/\hat{E}_{nt}$, for the six

TABLE 1.

Z_1	$r_{\hat{S}} = S_{n1}/S_{nt}$	$r_{\hat{E}} = \hat{E}_{n1}/\hat{E}_{nt}$
Boron	0.46	2.5
Carbon	0.55	2.3
Nitrogen	0.59	2.8
Oxygen	0.61	3.0
Fluorin	0.66	1.7
Neon	0.61	2.7

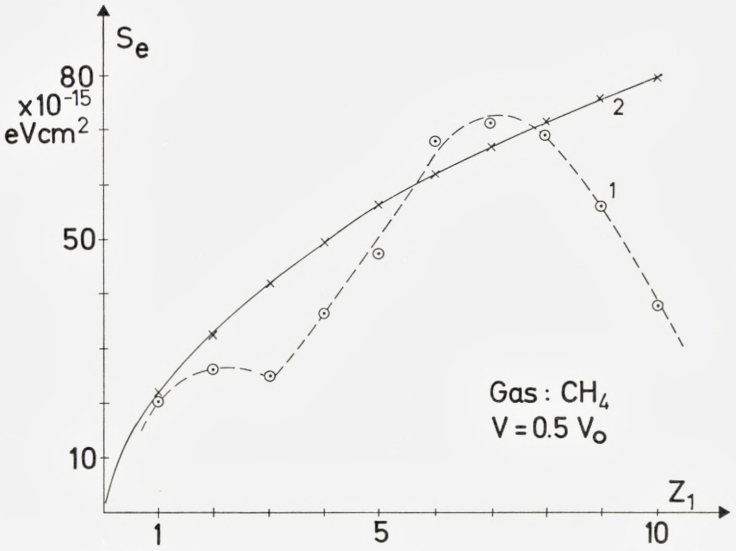

Fig. 15. Electronic stopping cross sections. 1 are the present experimental results and 2 the theoretical value from L.S.S.[3].

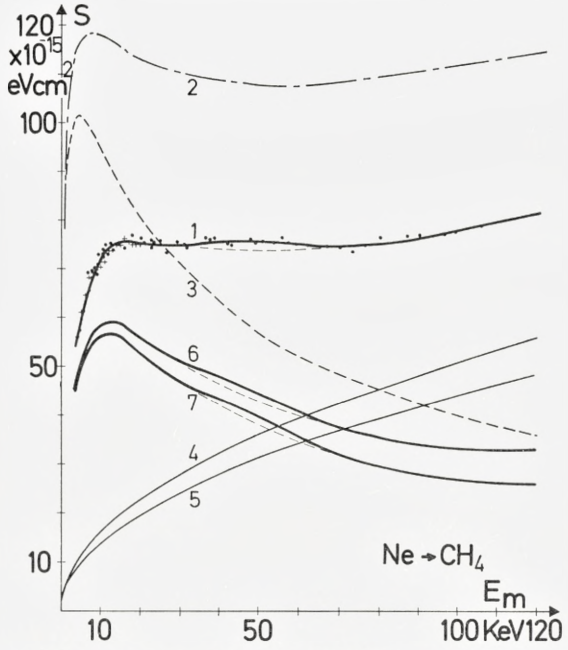

Fig. 16. Deduction of the pure nuclear stopping cross section. The curves are: 1, experimental total stopping S_x; 2, theoretical total stopping S_t, 3, theoretical nuclear stopping S_{nt} from L.S.S.[3]; 4 and 5, reduced theoretical electronic stopping curves S_{e_1} and S_{e_2}, respectively; 6 and 7, experimental nuclear stopping curves S_{n_2} and S_{n_1}, obtained from curve 1 by subtracting S_{e_2} and S_{e_1}, respectively.

heaviest elements, which were measured. The experimental maximum values of S_n are about half the theoretically predicted, and the maxima are experimentally found to lie at energies from two to three times higher than theoretically predicted.

To take into account possible systematic errors, the uncertainty in the S_e-value and in determining the exact position of the maximum, we estimate uncertainties of the order of $\pm 30\ ^0/_0$ for $r_{\hat{S}}$ and $r_{\hat{E}}$.

No correction for the difference between the projected range and the actual path length was applied. It should be pointed out, that therefore the difference between the theoretical and the measured values of the stopping cross sections, especially in the low energy range, may be expected to be even larger.

In the paper preceding L.S.S.[3] (Notes on Atomic Collisions I)[32] stopping cross section curves for three screened Coulomb potentials were given. In addition to the curve corresponding to the THOMAS-FERMI potential, which was chosen in the further development of the stopping theory, curves corresponding to a LENZ-JENSEN potential and a BOHR potential were given, (figure 7, Ref. 32). Comparing them to the THOMAS-FERMI curve, in the same way as the experimental results, they are both found to have $r_{\hat{S}}$ values of about 0.88, and the LENZ-JENSEN curve has $r_{\hat{E}} = 1.6$ and the BOHR curve has $r_{\hat{E}} = 2.5$.

Unpublished stopping power measurements by HVELPLUND[33] and recent range measurements by NEILSON et al[34] in the ε-range in which the nuclear stopping is dominating, also suggest that the nuclear stopping is overestimated by L.S.S.[3] and that the application of an other potential will give a better agreement between theory and experiment.

11. Conclusion

By applying the proportional detector technique, stopping cross section measurements were extended to very low energies and nearly all the problems connected with the fractionization effects and partly the problem connected with the recoil effect were solved.

The obtained complex results show that an extension of the measurements would be highly interesting, especially by using noble gases as stopping media and heavier ions as particles.

Acknowledgements

I would like to thank first of all FIN HANSEN, who, with great skill and care, has operated the accelerator and the equipment. Furthermore J. R. MACDONNALD and E. STRØMBERG for their help with the testing and the calibration of the detector. I am much indebted to J. LINDHARD and K. O. NIELSEN for inspiring discussions and to P. SIGMUND for valuable comments.

The Niels Bohr Institute
University of Copenhagen
Copenhagen, Denmark

Indleveret til Selskabet den 24. oktober 1973.
Færdig fra trykkeriet den 2. juli 1974.

References

1 N. Bohr, Mat-fys. Medd. Dan. Vid. Selsk. **18**, 8, (1948).
2 J. Lindhard and M. Scharff, Phys. Rev. **124**, 128, (1961).
3 J. Lindhard, M. Scharff and H. E. Schiøtt, Mat.-fys. Medd. Dan. Vid. Selsk. **33**, 14, (1963).
4 J. H. Ormrod and H. E. Duckworth, Can. J. Phys., **41**, 1424, (1963).
5 J. H. Ormrod, J. R. Macdonald and H. E. Duckworth, Can. J. Phys., **43**, 275, (1965).
6 P. Hvelplund, Mat-fys. Medd. Dan. Vid. Selsk. **38**, 4, (1971).
7 G. Högberg, Phys. Stat. Sol. (b), **48**, 829, (1971).
8 G. Sidenius, Proc. 3rd Conf. Physics of Electr. and Atomic Collisions, London 1963, p. 709.
9 P. Zahn, Z. Physik, **172**, 85, (1963).
10 D. Marx, Z. Physik, **195**, 26, (1966).
11 D. H. Poole, A. G. Warner, R. Hancock and R. L. Woolley, Journ. Physics D, **1**, 309, (1968).
12 R. Hancock, A. G. Warner and R. Woolley, Journ. Physics D, **2**, 991, (1969).
13 G. Högberg, Phys. Letters, **35**A, 327, (1971).
14 Proc. Second Int. Conf. on Beam Foil Spectroscopy, Nucl. Instr. and Meth., **90**, (1970).
15 S. K. Allison, J. Cuevas and M. Garcia-Munos, Phys. Rev. **127**, 792, (1962).
16 M. W. Thomson, Phil. Mag., **18**, 377, (1968).
17 G. Sidenius, Journ. Physics E, **2**, 657, (1968).
18 G. Sidenius, Journ. Physics E, **4**, 771, (1971).
19 G. Sidenius, Nucl. Instr. and Meth., **96**, 1, (1971).
20 J. R. Macdonald and G. Sidenius, Phys. Let., **28**A, 543, (1969).
21 K. O. Nielsen and O. Skilbreid, Nucl. Instr. and Meth., **2**, 15, (1958).
22 G. Sidenius and O. Holck, Proc. 8th Int. Conf. Low Energy Ion Acc. and Mass Separators, Sweden, 1973.
23 G. Sidenius, Proc. Int. Conf. Electromagnetic Isotope Separators., Marburg 1970, p. 423.
24 J. A. Dennis, Radiation Effects, **8**, 87, (1971).
25 J. A. Dennis, A.E.R.E.-Report – M – 2346.
26 H. K. Reynolds, D. N. F. Dunbar, W. A. Wenzel and W. Whaling, Phys. Rev. **92**, 742, (1953).
27 J. T. Park and E. J. Zimmerman, Phys. Rev. **131**, 1611, (1963).
28 S. Hughes, Phys. Med. Biol., **12**, 565, (1967).
29 J. T. Park, Phys. Rev. **138**, A1317, (1965).
30 Y. A. Teplova, V. S. Niclaev, I. S. Dmitriev and L. N. Fateeva, Sov. Phys. JETP, **15**, 31, (1962).
31 J. H. Ormrod, Can. J. Phys. **46**, 497, (1968).
32 J. Lindhard, V. Nielsen and M. Scharff, Mat-fys. Medd. Dan. Vid. Selsk. **36**, 10, (1968).
33 P. Hvelplund, private communications.
34 G. W. Neilson, B. W. Farmery and M. W. Thompson, Phys. Let., **46**A, 45, (1973).